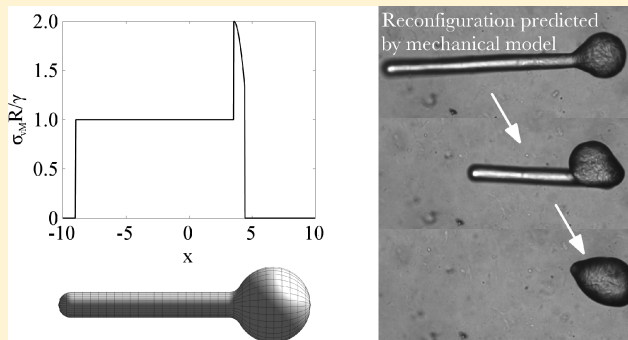


Model of Structured Emulsion Droplet Stability and Reconfigurability

Alexandra V. Bayles,^{†,‡} Tamás A. Prileszky,^{‡,§} Patrick T. Spicer,[§] and Eric M. Furst^{*,†,‡}[†]Department of Chemical Engineering, University of California, Santa Barbara, California 93106, United States[‡]Department of Chemical and Biomolecular Engineering, University of Delaware, Newark, Delaware 19716, United States[§]School of Chemical Engineering, University of New South Wales, Sydney, New South Wales 2052, Australia

ABSTRACT: A model of internally structured emulsion droplets is presented that accounts for the traction forces generated by interfacial tension and the von Mises yield criterion of the internal supporting network. For symmetric droplets, the method calculates the total stress acting on a droplet locally, allowing droplet stability and location of failure to be predicted. It is not regions of high interfacial curvature that prompt droplet reconfiguration, rather regions transitioning from high to low curvature. The model enables the design of emulsion droplet response and reconfigurability to external triggers such as changes in surface tension (surfactant concentration) and temperature.



1. INTRODUCTION

New classes of active and responsive materials include colloidal “swimmers,” which move, swarm, and assemble in the presence of a chemical signal,¹ Janus particle assemblies that contract and expand in response to an electric field,² polymer films that fold and unfold,³ and anisotropic fluids that detect the presence of toxins.⁴ Such materials are defined by a unique response to external chemical, physical, or thermal triggers. Their design provides new means to create composite materials and devices such as artificial muscles, “soft robotics,” cargo delivery vehicles, and environmental sensors.⁵

Structured and anisotropic emulsions are among this class of emerging responsive materials and exploit shape to enhance delivery mechanisms and efficiency.^{6–9} For instance, endoskeletal emulsions comprise a liquid dispersed phase with an entrained network of crystallites that intercalate to create an elastic structural framework. As a result, the droplets can be formed with a variety of anisotropic shapes using arrested coalescence, capillary-assisted molding, or microfluidic devices.^{10,11} These shapes, which range from spherocylinders to toroids, each have distinct distributions of Laplace pressures across their interfaces. This nonuniform pressure is an important consideration because it dictates the assembly of adsorbed surfactants and particles,^{12,13} their tendency to collide with and adsorb to surfaces, and the ability to reconfigure in response to environmental triggers, such as a change in temperature or surfactant concentration.

In this paper, we describe a model of the mechanical stability of internally structured anisotropic emulsions, including interfaces with concave regions. This builds upon previous work by Caggioni and co-workers who related the end-cap radius of spherocylindrical droplets to their stability.¹⁰ We propose a more sophisticated model to predict the stability and reconfiguration behavior of endoskeletal droplets with shapes that cannot be

described by a single radius.^{14,15} The approach developed here uses the von Mises yield criterion that incorporates stress information across an interface to predict the curvature-mediated interfacial pressure and internal network stresses of both experimental and theoretical endoskeletal droplets. The results provide insight into the structure and stability of shaped emulsion droplets¹⁶ and bicontinuous fluid networks,¹⁷ valuable information for designing nonspherical emulsions with tunable stability and responsiveness to external stimuli.

2. METHODS

The pressure difference between two fluids separated by an interface is a function of the interfacial tension and local curvature. The Young–Laplace equation

$$\Delta P = P_a - P_b = 2\gamma H = \gamma \left(\frac{1}{R_1} + \frac{1}{R_2} \right) \quad (1)$$

predicts the pressure difference across the interface, assuming the fluids are at rest, their interface is vanishingly thin, and the surface tension is constant.¹⁸ In eq 1, P_a and P_b are the pressures of the interior and exterior fluids, respectively; γ represents the surface tension; H is the mean curvature; and R_1 and R_2 are the local radii of curvature directed along the principal axes of curvature e_1 and e_2 . For an endoskeletal droplet, fluid a is the hydrophobic, dispersed phase constituting the droplet and fluid b is the hydrophilic, continuous phase, as shown in Figure 1. Figure 1 also demonstrates that the two radii of curvature are directed along orthogonal vectors.

If the mean curvature of the interface is positive, the pressure of the dispersed phase is greater than that of the continuous phase. As a result, the interface applies a compressive force on the droplet, fluid a . In the case of negative mean curvature, the pressure is directed into fluid b .

Received: February 10, 2018

Revised: March 16, 2018

Published: March 20, 2018

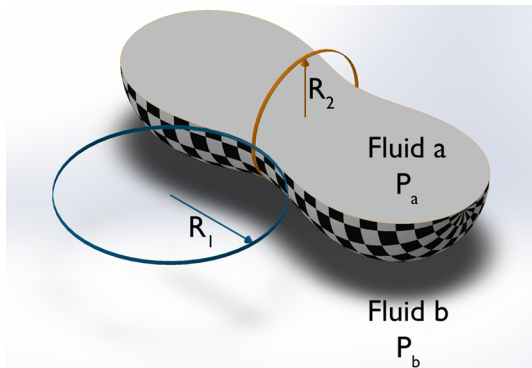


Figure 1. Schematic of nomenclature used to describe anisotropic droplet curvature. Fluids *a* and *b* are the droplet and continuous phase, respectively, and P_a and P_b are the pressures in the respective phases. R_1 and R_2 are the radii of curvature directed along the principal axes of curvature at a given point.

When a droplet is deformed, the mismatch of Laplace pressure across the interface causes a pressure gradient in the droplet; viscous droplets relax this pressure gradient by reshaping to form a sphere, which is the shape of minimum surface area for a given volume. By contrast, an endoskeletal droplet resists an interfacially driven deformation owing to its internal network. The network has a yield stress and stores the force of the pressure gradient elastically. As a result, endoskeletal droplets can retain anisotropic shapes, provided that the yield stress exceeds the stress gradient in the droplet.

The curvature on an anisotropic droplet interface varies spatially. The surface S that describes a droplet interface in \mathbb{R}^3 is parametrized by two variables u and v . \mathbf{r} describes the vector between the origin of the Cartesian coordinate system to a point (x, y, z) on S with direction components \mathbf{i} , \mathbf{j} , and \mathbf{k} . S is described by the equation

$$\mathbf{r}(u, v) = \phi(u, v)\mathbf{i} + \psi(u, v)\mathbf{j} + \xi(u, v)\mathbf{k} \quad (2)$$

where ϕ , ψ , and ξ are functions¹⁹ of the parameters u and v . The normal vector of the surface S with respect to the internal phase *a* is directed into fluid *b* and is defined as $\mathbf{n} = \frac{\mathbf{r}_u \times \mathbf{r}_v}{\|\mathbf{r}_u \times \mathbf{r}_v\|}$, where the subscript on \mathbf{r} denotes the first derivative with respect to the independent parameter, as $\mathbf{r}_i = \frac{\partial \mathbf{r}}{\partial i}$. The mean curvature of S is defined as half the negative of the divergence of the normal vector, $2H = -\nabla \cdot \hat{\mathbf{n}}$.

These definitions lay the framework for calculating the surface tension force \mathbf{t} at all points on a droplet surface using

$$\mathbf{t}(u, v) = -2\gamma H(u, v)\hat{\mathbf{n}}(u, v) \quad (3)$$

with surface parameters u and v . In addition, the vector definition demonstrates that the surface tension force is directed normal to the interface; whether the vector is directed toward fluid *a* or *b* depends on the sign of H .

A gradient in the external surface tension force due to variation in the surface curvature leads to a gradient in internal stress. Mapping this internal stress identifies regions prone to shape change, which is critical to the development of designer emulsions. The Euler–Cauchy stress principle forms the theoretical framework for internal stress mapping, stating that the internal and external forces acting on a continuous material must balance at mechanical equilibrium.²⁰ The network supporting an endoskeletal droplet interface comprises crystallites that are sufficiently small and uniformly distributed that the continuum approximation is satisfied. Specifically, the stress acting on an internal surface with normal \mathbf{i} is equal to the surface tension force integrated over a connected external surface S divided by the internal surface area A_i ,

$$\sigma_{ij} = \frac{F_j}{A_i} = \frac{\int t_j dS}{A_i} \quad (4)$$

Here, j denotes the component of the surface tension vector and corresponding stress in that direction. Depending on the orientation of the internal forces and area over which they are applied, nine stress components exist for a single differential element. These local components are described by the Cauchy stress tensor²¹

$$\boldsymbol{\sigma}_c = \begin{bmatrix} \sigma_{xx} & \sigma_{xy} & \sigma_{xz} \\ \sigma_{yx} & \sigma_{yy} & \sigma_{yz} \\ \sigma_{zx} & \sigma_{zy} & \sigma_{zz} \end{bmatrix} \quad (5)$$

The Cauchy stress tensor is useful for characterizing an isotropically yielding body. In the simplest sense, a body under load begins deforming plastically when the deformation becomes irreversible. The load that marks the transition from reversible, elastic to irreversible, plastic deformation is the yield strength Y , which is a positive scalar. To compare this scalar strength to the directional stress tensor, it is necessary to transform the tensor such that it is oriented in the direction of maximum compressive or tensile stress. The transformed tensor is the principal stress tensor

$$\boldsymbol{\sigma}_p = \begin{bmatrix} \sigma_1 & 0 & 0 \\ 0 & \sigma_2 & 0 \\ 0 & 0 & \sigma_3 \end{bmatrix} \quad (6)$$

The principal stresses σ_i are the eigenvalues of $\boldsymbol{\sigma}_c$; the principal planes on which they act are oriented by the eigenvectors of $\boldsymbol{\sigma}_c$.²²

Comparing the scalar yield strength with the principal stress tensor requires a yield surface X , described by

$$X = \Phi(\sigma_i) - K = 0 \quad (7)$$

Here, $\Phi(\sigma_i)$ is a function of the principal stress and K is a material constant related to the critical uniaxial yield strength Y_{1D} , typically through a scaling factor. When $\Phi(\sigma_i) < K$, the material deforms elastically, whereas when $\Phi(\sigma_i) > K$, the material deforms plastically. Thus, $\Phi(\sigma_i)$ represents a *yield criterion*. The yield criterion is valid for purely elastic materials; endoskeletal droplets, however, are viscoelastic. Certainly, a σ_{vM} stress that approaches the yield criterion without surpassing it may cause creep deformation of the droplets. However, droplets observed over several hours have not deformed substantially, suggesting that creep occurs over longer time scales than are experimentally accessible.

A yield criterion suitable to predict the stability of endoskeletal droplets is the von Mises yield criterion:²²

$$\sigma_{vM}(\sigma_i) = \sqrt{\frac{(\sigma_1 - \sigma_2)^2 + (\sigma_1 - \sigma_3)^2 + (\sigma_3 - \sigma_2)^2}{2}} \quad (8)$$

A zero σ_{vM} does not necessarily indicate zero stress; rather, it may arise from a uniform stress in all directions as occurs in spheres. When σ_{vM} exceeds the von Mises yield strength K_{vM} of the droplet internal network, an endoskeletal droplet is expected to deform. This stability criterion can be written instead as an expression,

$$\text{Stable: } \forall w \rightarrow \frac{\sigma_{vM}(\sigma_i(w))}{K_{vM}} \leq 1 \quad (9)$$

$$\text{Unstable: } \frac{\sigma_{vM}(\sigma_i(w))}{K_{vM}} > 1 \quad (10)$$

K_{vM} defines the yield strength of a material as calculated using the von Mises yield criterion model. It is an approximation of the material yield stress σ_y . Equation 9 confirms that larger yield stresses correspond to greater stability.

The stability criterion given in eq 10 is applicable for all anisotropic droplets. In practice, the analysis simplifies for droplets with three or more planes of symmetry, which then set the orientation of principal planes for all internal elements. When symmetric tension vectors are integrated across planes of symmetry, the shear components of the Cauchy stress tensor $\sigma_{ij, i \neq j}$ vanish. The average principal stress tensor

can be evaluated directly for internal segments, which lie orthogonal to planes of symmetry.

In the following, we calculate the von Mises stress criteria for endoskeletal droplet shapes, which can be realized in experiments. Specifically, we define axisymmetric droplets by the parametric equation

$$\mathbf{r}(u, v) = f(u)\cos(v)\mathbf{e}_i + g(u)\mathbf{e}_j + h(u)\sin(v)\mathbf{e}_k \quad (11)$$

where $f(u)$ and $g(u)$ are analytical functions that describe the droplet profile. Using computational software (e.g., Mathematica, Maple), the principal stresses on an internal segment oriented along \mathbf{e}_j can be evaluated directly by independently integrating components of the tension vector, as in

$$\sigma_i(w) = \sigma_{ii}(w) = \frac{\mathbf{F}_i}{A_i(w)} = \frac{\int \int_{w_0(u,v)}^{w_1(u,v)} \mathbf{t}_i \, dS}{A_i} \quad (12)$$

Here w indicates a point along the axis of symmetry \mathbf{k} ; w_0 and w_1 designate the bounds of the connected surfaces. The variables w_0 and w_1 map to (u, v) space such that translating between (u_0, v_0) to (u, v) defines the entire surface. This method of integration and its relationship to w is demonstrated in Figure 2 for an axisymmetric doublet similar in shape to two coalescing spherical droplets.¹⁵

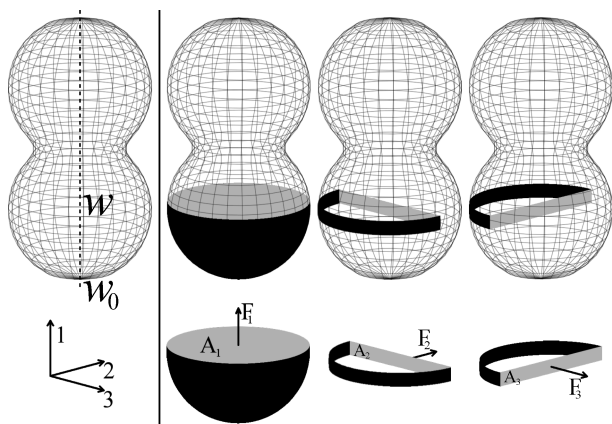


Figure 2. Integrating across connected surfaces to find the principal stresses on a segment (in gray) at position w . For each of the principal stresses, the associated surfaces of integration are shown in black. The areas A_i bounded by the connected surface are also marked. w_0 pertaining to the second principal axis is also included.

For such axisymmetric droplets, $\sigma_2 = \sigma_3$. The von Mises yield criterion simplifies to

$$\sigma_{\text{VM}}(\sigma_i(w)) = |\sigma_1(w) - \sigma_2(w)| \quad (13)$$

This yield criterion is evaluated at every point w along the axis of symmetry.

Droplets with three planes of symmetry require that the yield criterion be calculated along the intersection of any two planes of symmetry. Thus, where a single profile adequately describes the internal stress distribution of a rotationally symmetric droplet, droplets with three axes of symmetry require three separate profiles. For segments that lie orthogonal to these axes, eq 12 determines σ_p , and eq 8 determines $\sigma_{\text{VM}}(\sigma_i(w))$ since σ_2 does not necessarily equal σ_3 .

3. RESULTS AND DISCUSSION

3.1. Rotationally Symmetric Droplets. The von Mises yield criterion can be calculated for any solid of revolution, provided the axis of revolution intersects the rotated surface, e.g., dumbbells, rods, and spherocylinders. Other shapes, such as toroids require a generalized three-dimensional calculation that is outside the scope of this paper. In Figure 3, calculations of the

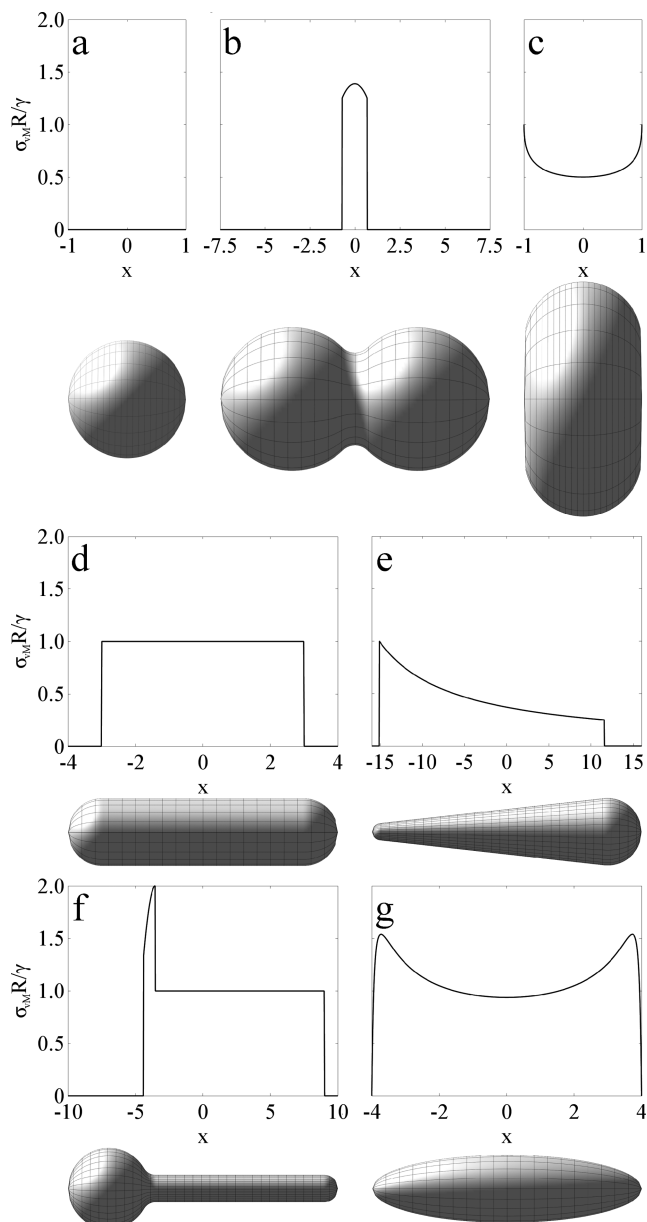


Figure 3. Internal stress distributions calculated using Mathematica for a variety of solids of revolution normalized by $\frac{\gamma}{R}$, where R is a characteristic radius of the solid. The abscissa marks the position on the solid relative to the characteristic radius. Each plot represents the stress distribution of the shape immediately beneath it: a is for a sphere of radius R ; b shows two partially coalesced spheres of radius $4R$ and a neck region curving with radius R forming a dumbbell; c is a disk of radius $3R$ and depth of $2R$; d is a spherocylinder with spherical end-caps of radius R ; e is a cone with end-caps of R and $4R$; f is a ball-and-stick with a sphere of radius $3R$ joined with a spherocylinder of radius R ; and g is an ellipsoid with semiminor axis R and semimajor axis $4R$.

internal stress distribution on a variety of shapes are shown. Each shape in Figure 3 can be created experimentally; spheres are the native droplet shape, and 3b results from forcing two spheres to coalesce.¹⁵ The droplet in 3c can be produced in microfluidic devices, and 3d,e,f can be formed by capillary molding.^{10,11} By using magnetic fields or by stretching in an elastic matrix,²³ ellipsoidal droplets as in 3g are also possible.

The results of the model calculations in Figure 3 reveal several key factors about the stability of anisotropic endoskeletal

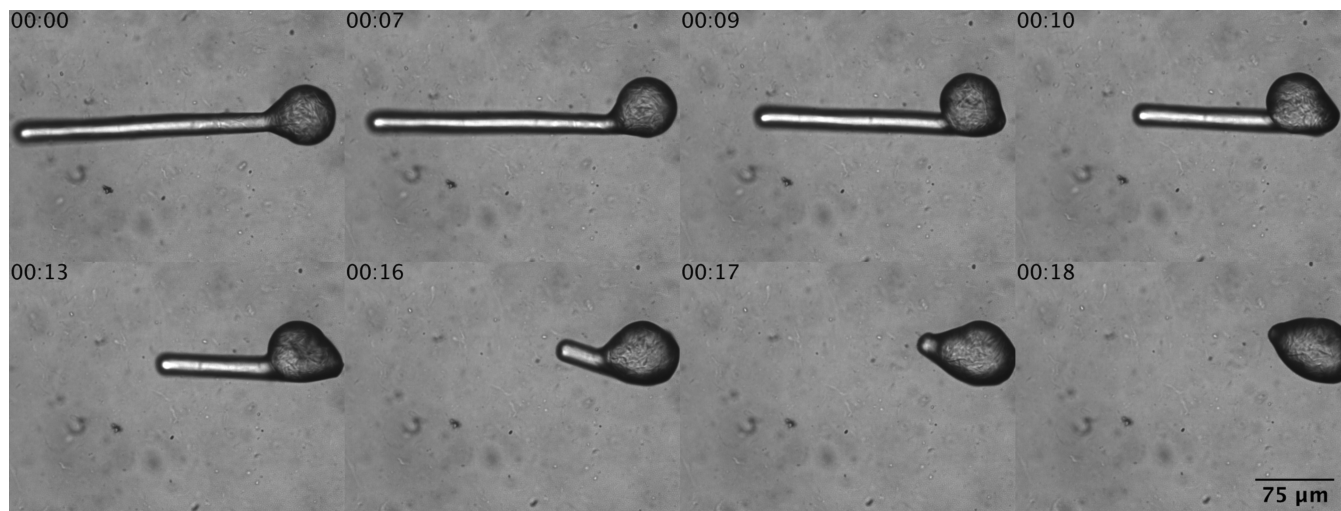


Figure 4. Endoskeletal ball-and-stick droplet responding to heating. As the temperature rises, the droplet internal network weakens, reducing its yield stress and, thus, the interfacial stress it can support. The droplet responds by reshaping to minimize the interfacial stress acting on the internal network. Initial failure of the droplet internal network occurs at the inversion of curvature between the ball-and-stick, where the von Mises yield criterion is at a maximum.

droplets. First, any region of a droplet that is locally spherical, as in the end-caps of a spherocylinder or cone, does not have a von Mises stress. Depending on the curvature outside the spherical region, different internal stress distributions result. In a droplet with a cross-section of uniform area, the stress distribution remains constant as the stress exerted by the end-caps is evenly distributed throughout the interior as in 3d. Here, the uniform stress scales with γ/R , which is copacetic with previous experimental results. Specifically, Caggioni et al. showed that rod shaped droplets of varying sizes and crystallite content are stable when $\sigma_y > 2\gamma/R$, where σ_y is the network yield strength.¹⁰ Moreover, this scaling quantitatively predicts the reconfiguration triggered by a temperature increase (decrease in σ_y)¹¹ or dilution (increase in γ).¹⁰ As droplet area increases, for instance moving from left to right in the cone in Figure 3e, the internal stress decreases due to the decreasing gradient in curvature.

From these insights, it is possible to predict where in the droplet structure a reconfiguration event is likely to begin. For example, a disk droplet will change shape by pushing the flat edges out, noted by the high von Mises stress near the flat end-caps. This shape change progresses until the surface tension is balanced by the internal elasticity of the internal network, either when the droplet is a sphere or at an intermediate shape between discoid and spherical. An ellipsoidal droplet fails by collapsing first near the ends, where curvature is high, and proceeding toward the center until spherical or internal elasticity arrests further deformation. When a droplet transitions from a convex to a concave region, very large internal stresses can result where local principal curvatures have opposite signs, noted in both Figure 3b,f.

The source of the large internal stress in droplets with opposing curvature is clear when considering eq 13. In the case of a sphere, σ_1 and σ_2 are equal because the curvature is equal, and the resulting stress is directing inward at all locations. As a result, the two terms cancel to produce a net zero internal stress. However, in the case of a saddle, σ_1 and σ_2 are of opposite signs; one is directed inward and the other outward. Correspondingly, the two terms are additive, increasing the maximum internal normalized stress to a value greater than unity. For the dumbbell and ball-and-stick of Figure 3, the large internal stress acts to

force the concave region outward until the entire surface is a convex sphere.

Experimentally, reconfiguration occurs at interfacial saddle points. Saddle points form where an endoskeletal droplet wets an obstacle (e.g., bubbles, fibers,¹¹ or other droplets¹⁰), causing the droplet to deform by wrapping around the obstacle. Discrete anisotropic droplets reconfigure at the point of greatest stress on their own interface. Figure 4 shows an oil-in-water ball-and-stick droplet produced via capillary molding using the materials and procedure described by Caggioni et al.¹⁰ Briefly, a crystalline droplet is melted at 60 °C, partially aspirated into a capillary, and recrystallized at 25 °C. The droplet is then ejected from the capillary and its crystalline internal network supports the anisotropic interface. Reconfiguration is driven by heating the emulsion to 60 °C to weaken the network; when the droplet yield stress σ_y falls below the von Mises stress σ_{vM} , the droplet collapses. As the internal stress distributions of Figure 3f predict, the junction between ball-and-stick experiences the greatest stress and collapses first. The effects of this stress are apparent by the second panel of Figure 4. Here, the ball perpetuates a concave region by “rolling” toward the stick region until it reaches the stick end-cap, ultimately eliminating concavity entirely.

Combining the von Mises yield criterion calculation with a simple experiment that tracks the coalescence of two spherical droplets as in Figure 3b provides yield stress information about the internal network of an endoskeletal droplet. Previously, Pawar and co-workers demonstrated that the coalescence between two viscoelastic spheres allows the elastic modulus of the droplet to be calculated from the strain induced by interfacial tension.¹⁵ By mapping the internal stress throughout the droplet doublet, the von Mises yield criterion calculation provides a model that predicts the yield stress of the droplet structure. Here, a useful definition for the yield stress is the point at which the interfacial tension can no longer pull the two spheres closer together and coalescence stops; certainly this is a dynamic definition of the yield stress and does not necessarily reflect the static yield stress of a droplet that has not been deformed through arrested coalescence. However, the dynamic definition provides a better estimate of the true yield stress present in an experimental

droplet than can bulk shear rheology experiments, which find the yield stress under pure shear.¹¹

In Figure 5, the dimensions of a droplet doublet are calculated by preserving the volume of two spheres while requiring the neck

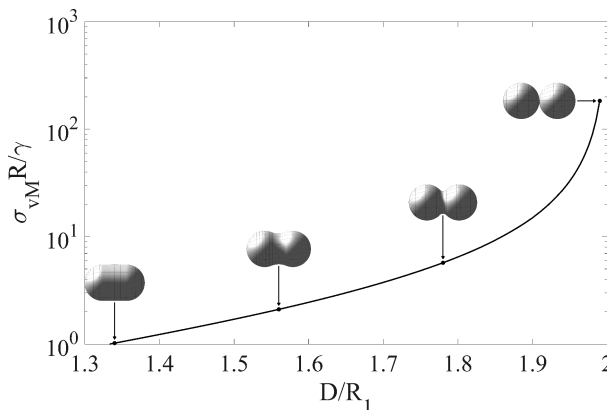


Figure 5. Required normalized yield stress to arrest coalescence of two spherical droplets as a function of the distance between droplet centers normalized by droplet radius.

region between droplets to have a radius tangent to the coalescing spheres. The resulting shapes closely mimic those of previous studies.¹⁵ Indeed, using the coalescence behavior from Pawar, we find that the yield stress of petrolatum-hexadecane mixtures used to create endoskeletal droplets is on the order of 100 Pa for droplets with more than 40% petrolatum by weight. This value of K_{vM} agrees with yield stress measurements obtained from rotational rheometry¹¹ when using a surface tension value typical for an endoskeletal droplet system. The surface tension experienced by these droplets falls in the range of 1.5 and 10 mN m⁻¹ measured for SDS-laden interfaces of low petrolatum fraction and pure hexadecane,²⁴ respectively. Using the von Mises yield criterion thus enables two experiments—arrested coalescence between two droplets and pendant-drop measurements of surface tension—to predict the yield stress of internally structured emulsion droplets.

Previous work details the density and crystallization kinetics of the network.²⁵ The component crystallites of the network range from 1–5 μm—significantly smaller than the dimensions of a typical droplet—and decrease in size for faster crystallization rates. Because the von Mises yield criterion describes the behavior of a homogeneous, elastic material and the K_{vM} agrees closely with experimental values of σ_y , the current study suggests that the network of crystallites within an endoskeletal droplet can be approximated as a continuum. Certainly, this approximation may not hold for small droplets with dimensions that approach the length scale of the crystallites. However, a decrease in droplet size is accompanied by an increase in temperature control, allowing droplet quench rate to be tuned to decrease crystallite size further.²⁵ Regardless, caution should be exercised when applying the von Mises yield criterion to a droplet geometry with structural components approaching the dimensions of the droplet itself.

3.2. Reflectively Symmetric Droplets. Performing the same calculation on a droplet with three axes of symmetry provides additional control over the shape of droplets and confirms some insights gained from studying rotationally symmetric droplets. Droplets produced in a microfluidic device

can be approximated as flattened spherocylinders,¹⁴ which share characteristics of superquadrics obeying the functional form

$$1 = \left(\frac{x}{R_x}\right)^4 + \left(\frac{y}{R_y}\right)^2 + \left(\frac{z}{R_z}\right)^4 \quad (14)$$

and triaxial ellipsoids of the form

$$1 = \left(\frac{x}{R_x}\right)^2 + \left(\frac{y}{R_y}\right)^2 + \left(\frac{z}{R_z}\right)^2 \quad (15)$$

While the curvature is only a rough approximation (more detailed, fourth-order polynomials provide a closer fit to the actual droplet shape at the cost of high computational complexity and Runge oscillations), the von Mises yield criterion calculated through a droplet reveals where droplets are most susceptible to reconfiguration. The stress profiles in Figure 6 demonstrate that

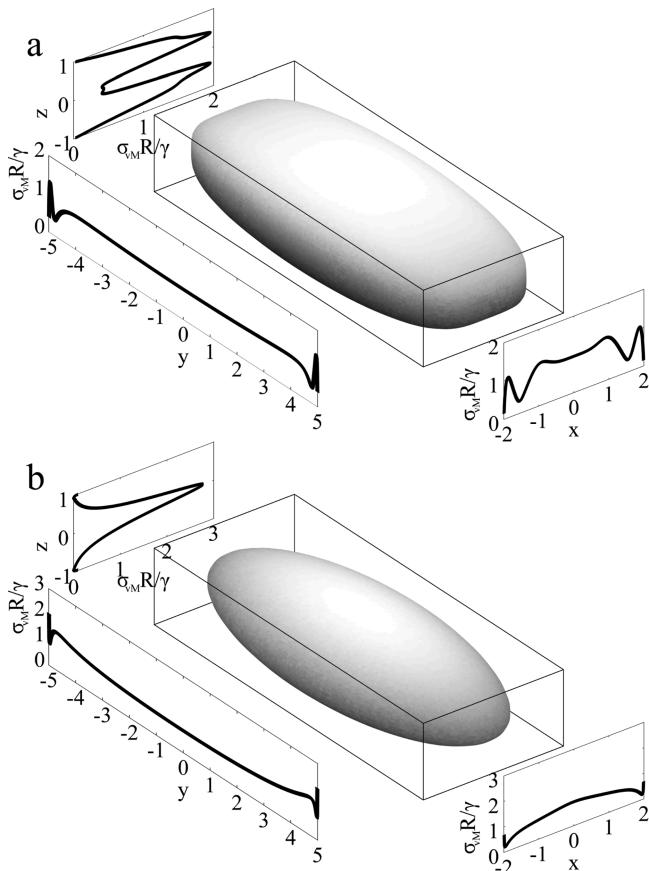


Figure 6. Superquadric and ellipsoidal approximations of an endoskeletal droplet with the normalized von Mises yield criterion calculated across each plane of symmetry. The end-caps, where there are rapid changes in curvature, are subject to large stresses, indicating that these are the regions most susceptible to shape change.

droplet end-caps are subject to the largest von Mises stresses, which reflects the rapid transition between high- and low-curvature regions of the droplet interface. This behavior is clear in both ellipsoidal and superquadric shapes, which suggests the same is likely true of the flattened spherocylinder shape droplets produced in microfluidics.¹⁴

4. CONCLUSIONS

A calculation of the internal stress distribution combined with the von Mises yield criterion informs the design of new shaped emulsions and improves our understanding of droplets that are already produced. Modeling symmetric droplets using parametric and implicit surface functions recovers experimentally observed modes of reconfiguration. While this approach works well for symmetric droplets, calculations become more difficult for droplets with general three-dimensional surfaces that cannot be reduced to an analytical profile. For this, accurate numerical representations of surfaces should enable calculation of the full Cauchy stress tensor and internal stress distribution. Values of stress provided by the calculations allow material properties, such as droplet yield stress, to be determined and new stable and responsive emulsion shapes to be conceived, such as droplets that can fold into intermediate structures before completely collapsing to a sphere.¹⁶ Alternative approaches to generating nonspherical interfaces, such as bijels^{26,27} or Pickering emulsions,^{28,29} have similarly curved surfaces to endoskeletal droplets; the calculations and analyses presented here can be extended to these materials to describe and predict their stability and reconfiguration behavior, as well.

■ AUTHOR INFORMATION

Corresponding Author

*E-mail: furst@udel.edu.

ORCID

Tamás A. Prileszky: [0000-0003-3314-6690](https://orcid.org/0000-0003-3314-6690)

Patrick T. Spicer: [0000-0002-8562-3906](https://orcid.org/0000-0002-8562-3906)

Author Contributions

A.V.B. and T.A.P. contributed equally to this manuscript. E.M.F. and P.T.S. designed the research. A.V.B. and T.A.P. performed the research and analyzed the data. T.A.P., A.V.B., and E.M.F. wrote the paper.

Notes

The authors declare no competing financial interest.

■ ACKNOWLEDGMENTS

The authors would like to thank the National Science Foundation for funding (Grant Number CBET-1336132).

■ REFERENCES

- (1) Wang, W.; Duan, W.; Ahmed, S.; Sen, A.; Mallouk, T. E. From One to Many: Dynamic Assembly and Collective Behavior of Self-Propelled Colloidal Motors. *Acc. Chem. Res.* **2015**, *48*, 1938–1946.
- (2) Shah, A. A.; Schultz, B.; Zhang, W.; Glotzer, S. C.; Solomon, M. J. Actuation of shape-memory colloidal fibres of Janus ellipsoids. *Nat. Mater.* **2015**, *14*, 117–124.
- (3) Na, J. H.; Evans, A. A.; Bae, J.; Chiappelli, M. C.; Santangelo, C. D.; Lang, R. J.; Hull, T. C.; Hayward, R. C. Programming reversibly self-folding origami with micropatterned photo-crosslinkable polymer trilayers. *Adv. Mater.* **2015**, *27*, 79–85.
- (4) Lin, S.-Y.; Hsu, W.-H.; Lo, J.-M.; Tsai, H.-C.; Hsiue, G.-H. Novel geometry type of nanocarriers mitigated the phagocytosis for drug delivery. *J. Controlled Release* **2011**, *154*, 84–92.
- (5) Snezhko, A.; Aranson, I. S. Magnetic manipulation of self-assembled colloidal asters. *Nat. Mater.* **2011**, *10*, 698–703.
- (6) Spicer, P. T.; Caggioni, M.; Bayles, A. V.; Lenis-Abril, J. Shape-changing Droplet. European Patent EU2 909 299 B1, November 30, 2016.
- (7) Spicer, P. T.; Caggioni, M.; Bayles, A. V.; Lenis-Abril, J. Non-spherical Droplet. US Patent US9,597,648 B2, Mar 21, 2017.
- (8) Denkov, N.; Tcholakova, S.; Lesov, I.; Cholakova, D.; Smoukov, S. K. Self-shaping of oil droplets via the formation of intermediate rotator phases upon cooling. *Nature* **2015**, *528*, 392–395.
- (9) Haas, P. A.; Goldstein, R. E.; Smoukov, S. K.; Cholakova, D.; Denkov, N. Theory of Shape-Shifting Droplets. *Phys. Rev. Lett.* **2017**, *118*, 088001.
- (10) Caggioni, M.; Bayles, A. V.; Lenis, J.; Furst, E. M.; Spicer, P. T. Interfacial stability and shape change of anisotropic endoskeleton droplets. *Soft Matter* **2014**, *10*, 7647–7652.
- (11) Caggioni, M.; Lenis, J.; Bayles, A. V.; Furst, E. M.; Spicer, P. T. Temperature-Induced Collapse, and Arrested Collapse, of Anisotropic Endoskeleton Droplets. *Langmuir* **2015**, *31*, 8558–8565.
- (12) Cavallaro, M.; Botto, L.; Lewandowski, E. P.; Wang, M.; Stebe, K. J. Curvature-driven capillary migration and assembly of rod-like particles. *Proc. Natl. Acad. Sci. U. S. A.* **2011**, *108*, 20923–20928.
- (13) Lewandowski, E. P.; Cavallaro, M.; Botto, L.; Bernate, J. C.; Garbin, V.; Stebe, K. J. Orientation and self-assembly of cylindrical particles by anisotropic capillary interactions. *Langmuir* **2010**, *26*, 15142–15142.
- (14) Prileszky, T. A.; Furst, E. M. Fluid Networks Assembled from Endoskeletal Droplets. *Chem. Mater.* **2016**, *28*, 3734–3740.
- (15) Pawar, A. B.; Caggioni, M.; Hartel, R. W.; Spicer, P. T. Arrested coalescence of viscoelastic droplets with internal microstructure. *Faraday Discuss.* **2012**, *158*, 341–350.
- (16) Dahiya, P.; DeBenedictis, A.; Atherton, T. J.; Caggioni, M.; Prescott, S. W.; Hartel, R. W.; Spicer, P. T. Arrested coalescence of viscoelastic droplets: triplet shape and restructuring. *Soft Matter* **2017**, *13*, 2686–2697.
- (17) Lee, M. N.; Mohraz, A. Bicontinuous Macroporous Materials from Bijel Templates. *Adv. Mater.* **2010**, *22*, 4836–4841.
- (18) marquis de Laplace, P. S. *Traité de Mécanique Céleste*; Duprat: Paris, 1805; Vol. 4; pp 1–79.
- (19) Gray, A. *Modern Differential Geometry of Curves and Surfaces with Mathematica*, 2nd ed.; CRC Press: Boca Raton, FL, 1997.
- (20) Truesdell, C.; Toupin, R. *Principles of Classical Mechanics and Field Theory*; Springer-Verlag: Berlin, 1960; pp 226–858.
- (21) Ugural, A. C.; Fenster, S. K. *Advanced Mechanics of Materials and Applied Elasticity*, 5th ed.; Pearson Education: Upper Saddle River, NJ, 2012.
- (22) Roark, R. J. *Formulas for Stress and Strain*; McGraw-Hill: New York, 1943.
- (23) Nagy, M.; Keller, A. Ellipsoidal polymer particles with predesigned axial-ratio. *Polym. Commun.* **1989**, *30*, 130–132.
- (24) Oh, S. G.; Shah, D. O. Effect of counterions on the interfacial tension and emulsion droplet size in the oil/water/dodecyl sulfate system. *J. Phys. Chem.* **1993**, *97*, 284–286.
- (25) Prileszky, T. A.; Furst, E. M. Crystallization Kinetics of Partially Crystalline Emulsion Droplets in a Microfluidic Device. *Langmuir* **2016**, *32*, 5141–5146.
- (26) Clegg, P. S.; Herzig, E. M.; Schofield, A. B.; Horozov, T. S.; Binks, B. P.; Cates, M. E.; Poon, W. C. K. Colloid-stabilized emulsions: behaviour as the interfacial tension is reduced. *J. Phys.: Condens. Matter* **2005**, *17*, 3433.
- (27) Haase, M. F.; Stebe, K. J.; Lee, D. Continuous Fabrication of Hierarchical and Asymmetric Bijel Microparticles, Fibers, and Membranes by Solvent Transfer-Induced Phase Separation (STRIPS). *Adv. Mater.* **2015**, *27*, 7065–7071.
- (28) Pawar, A. B.; Caggioni, M.; Ergun, R.; Hartel, R. W.; Spicer, P. T. Arrested coalescence in Pickering emulsions. *Soft Matter* **2011**, *7*, 7710.
- (29) Bon, S. A. F.; Mookhoek, S. D.; Colver, P. J.; Fischer, H. R.; van der Zwaag, S. Route to stable non-spherical emulsion droplets. *Eur. Polym. J.* **2007**, *43*, 4839–4842.